Atomic structure and crystallographic shear planes in epitaxial TiO_2 anatase thin films

R. Ciancio,[1] A. Vittadini,[2] A. Selloni,[3] C. Aruta,[4] U. Scotti di Uccio,[4] G. Rossi,[1,5] E. Carlino[1]

[1]*CNR-IOM TASC Area Science Park, Basovizza 34149 Trieste, Italy*
[2]*CNR-ISTM and CR-INSTM "Village", c/o Department of Chemical Sciences, University of Padova, Italy*
[3]*Department of Chemistry, Princeton University, Princeton, NJ 08544, USA*
[4]*CNR-SPIN and Department of Physical Sciences, University of Napoli, 80126 Napoli, Italy*
[5]*Department of Physics, University of Milano, 20100 Milano, Italy*

Corresponding author: Regina Ciancio
CNR-IOM, TASC Laboratory Area Science Park, Basovizza S.S. 14 Km 163.5, 34149 Trieste, Italy
Tel. +39.040.375.6467 - Fax: +39.040.226767
E-mail: ciancio@iom.cnr.it

Summary
We report on the high resolution transmission electron microscopy (HRTEM) and high angle annular dark field scanning transmission electron microscopy (HAADF-STEM) study of TiO_2 anatase thin films grown by pulsed laser deposition on $LaAlO_3$ substrates. The analysis provides evidence of a peculiar growth mode of anatase on $LaAlO_3$ that is characterized by the formation of an epitaxial layer at the film/substrate interface. In particular, the film is split into two adjacent slabs of about 20 nm each, both displaying the same Bravais lattice compatible with the anatase tetragonal cell. The formation of two different families of crystallographic shear (CS) superstructures is observed within the film, namely (103)- and (101)-oriented CS plane structures, occurring in the outer film region and in proximity of the film/substrate interface, respectively. HAADF analysis and Energy Dispersive Spectroscopy highlight the occurrence of Al interdiffusion from the substrate into the film region. By combining HRTEM results, image simulation techniques and DFT calculations we determine the atomic structure of the CS planes, and show that they are cubic-TiO-based structures analogous to the Ti_nO_{2n-1} Magnéli phases derived from rutile.

Key words: anatase, composition, segregation, defects and impurities, HRTEM, HAADF.

Introduction

Transition metal oxides form a broad and diverse class of materials (Rao and Raveau, 1998; Henrich and Cox, 1994) in which TiO_2 holds a prominent role for its unique physico-chemical properties and promising technological applications, ranging from photocatalysis and solar energy conversion to electrodes for regenerative fuel cells and memresistor switching memories (Weinberger and Garber, 1995; Chen and Yang, 1993; Jellison *et al.*, 1997, Chen *et al.*, 2002; Szot *et al.*, 2011). The most common TiO_2 crystalline phases are rutile and anatase. Both structures can be described in terms of a tetragonal lattice where the basic building block consists of chains of distorted TiO_6 octahedra. Their physical and chemical behaviors show significant differences however (Ganduglia-Pirovano *et al.*, 2007). In particular, rutile is the thermodynamically stable bulk phase, whereas anatase is stable in nanomaterials and has a higher photocatalytic activity (Chambers, 2010). Over the last decades, extensive studies have been made to obtain thin film anatase single crystals via a variety of methods (Chambers, 2010; Chang *et al.* 1991; Murakami *et al.*, 2001; Yamamoto *et al.*, 2001; Lotnyk *et al.*, 2007; Weng *et al.*, 2008; Wang *et al.*, 2010) and on a wide variety of substrates, the choice of these last being of primary importance to obtain high quality thin films. Among all substrates used, $LaAlO_3$ (LAO) is considered an ideal candidate, because of the relatively small lattice mismatch (about 0.2%) (Murakami *et al.*, 2001; Yamamoto *et al.*, 2001; Lotnyk *et al.*, 2007; Weng *et al.*, 2008; Wang *et al.*, 2010; Kennedy and Stampe, 2003) that is a prerequisite to obtain anatase thin films of good crystalline quality with clean and sharp TiO_2/LAO heterointerfaces. To date, in spite of the impressive advances in the heteroepitaxial growth of TiO_2, a detailed understanding of the functional properties of the binary material is still

lacking, mainly because they are strongly related to the presence and type of defects. A systematic investigation of defects requires a careful characterization of microstructure and of local chemical properties both of the film and of the film/substrate interface. The interfacial microstructures of TiO_2/LAO have been previously investigated, (Murakami *et al.*, 2001; Weng *et al.*, 2008; Wang *et al.*, 2010); however, the understanding of the film growth modes is still far from being complete. In this context, high-resolution cross-sectional TEM provides a unique opportunity to ascertain the presence of structural defects at the atomic scale and to follow the evolution of the nanostructure across the growth direction.

In this work, we provide a full characterization of the nanostructure and of the type of defects in epitaxial anatase TiO_2 thin films grown on (001) LAO substrates. By resorting to cross-sectional high resolution transmission electron microscopy (HRTEM) and high angle annular dark field (HAADF) scanning TEM (STEM) analyses, we determine the nanostructural assessment of the TiO_2 films versus growth direction and draw conclusions on the role of atomic interdiffusion from the substrate towards the film. In particular, we show the existence of two different growth modes within the TiO_2 films resulting in the formation of two adjacent slabs characterized by two distinct Magnéli-like superstructures. By combining HRTEM experiments, HRTEM image simulation techniques, and density functional theory (DFT) calculations we determined the atomic structure of the two superlattices and investigated the thermodynamic stability of these superstructures as a function of the oxygen supersaturation during film growth.

Materials and Methods

TiO_2 films were deposited by pulsed laser deposition on (001) LAO substrate held at 700°C in a 10^{-1} mbar oxygen atmosphere. A KrF excimer laser beam (248 nm, 25 ns duration full width half maximum) was focused on a stoichiometric target with a fluence of $2 J \times cm^{-2}$. The growth process was monitored in situ by reflection high-energy electron diffraction (RHEED), by taking sequences of diffractions at different stages of the growth.

Cross-sectional samples in the [010] TiO_2 zone axis suitable for TEM/STEM analyses have been obtained by a conventional polishing technique followed by dimpling and ion milling. The ion mill process was performed following a well-established protocol to avoid preferential sputtering at the substrate/film interface (Carlino, 2008). TEM/STEM experiments were performed using a TEM/STEM JEOL 2010 UHR field emission gun microscope operated at 200 kV with a measured spherical aberration coefficient C_s=(0.47±0.01) mm. The microscope is equipped with an Oxford system for energy dispersive X-ray spectroscopy (EDS) studies. HAADF images were acquired using an illumination angle of 12 mrad and a collection angle $88 \leq 2\theta \leq 234$ mrad. HRTEM image simulations were performed by JEMS simulation package program (Stadelmann, 2006).

DFT calculations were performed using the Perdew-Burke- Ernzerhof (Perdew *et al.*, 1996) parametrization of the generalized gradient approximation (GGA), both without and with the inclusion of onsite Coulomb repulsion U on the Ti 3d states (Anisimov *et al.*, 1991). For the latter, the computed (Cococcioni and deGironcoli, 2005) value U = 3.5 eV was employed. We adopted the plane-wave pseudopotential scheme as implemented in the QUANTUM ESPRESSO package (Giannozzi *et al.*, 2009) with the computational setup extensively tested in Ref. (Marzari *et al.*, 1999) For the GGA+U calculations, we used the GGA-optimized lattice constants but reoptimized the internal degrees of freedom. More details on the calculations are in Ref (Ciancio *et al.*, 2012).

Results and Discussion

A representative overview of the TiO_2/LAO cross-sectional region is given in the bright field image of Figure 1a obtained under multi-beams conditions with the primary electron beam parallel to the [010] crystal direction of the film. From this figure, one can see that substrate surface is rather flat and it is entirely covered by the anatase TiO_2 for a thickness of about 40 nm, as expected from the deposition process. More interestingly, the bright field TEM image shows that the film is divided into two adjacent regions of about 20 nm thicknesses each (hereafter called I and II) running parallel to the [100] LAO crystallographic direction and characterized by different diffraction contrast. Diffractograms computed over several areas of the two regions reveal no differences between the Bravais lattice of I and II, both being compatible with the anatase

tetragonal cell. At a closer inspection, HRTEM shows that the two slabs are characterized by a modulated structure typical of the existence of crystallographic shear (CS) planes. In particular, two different groups of CS planes can be identified: majority CS planes with approximately 1.3-nm spacing and forming an angle ϕ_α=38° with the [100] direction, in the outer film region whereas minority planes having ~2.0 nm spacing and forming an angle ϕ_β=68° with [100], in proximity of the film/substrate interface. Diffractograms taken over the two CS regions and displayed in Figure 1c,d, respectively, show a typical multiple-peak pattern, which indicates a superstructure-like behavior originating from the CS planes in the film and defining two new superlattices. In each diffractogram, the distance between the spots [red and green arrows in Figure 1c,d, respectively] is strictly related to the 1.3- and 2.0-nm periodicity of the TiO_2-modulated structure. The arrowed peaks can thus be interpreted as satellite peaks of the d_{hkl} superlattices. The normal to the $(hkl)_A$ shear planes lies along the c^* direction of the new superlattices and it is given, for a phase Ti_nO_{2n-1}, by the relation $c^*=nd_{hkl}^*$.

Recurrent CS planes have been previously observed in slightly reduced TiO_{2-x} rutile systems and attributed to the occurrence of oxygen vacancies within the samples. In particular, at low concentration ($x<10^{-4}$) the oxygen vacancies are initially accommodated as point defects. At greater reduction, CS planes are formed and point defects eliminated. A great example is represented by the mixed-valence Ti_nO_{2n-1} Magnéli phases which are stable for intermediate stoichiometries between Ti_2O_3 and TiO_2 (Magnéli, 1978; Thomas, 1984). Available investigations on reduced TiO_{2-x} phases have generally focused on rutile, where Magnéli phases have been detected and extensively characterized both experimentally and theoretically (Bursill *et al.*, 1969; Bursill and Hyde, 1971; Anderson and Tilley, 1970; Bursill and Blanchin, 1984; Leonov *et al.*, 2006; Liborio and Harrison, 2008; Liborio *et al.*, 2009). The nature of similar CS structures in anatase is largely unknown, though experimental evidence of their existence has been reported previously (Chambers *et al.*, 2002b). Starting from the HRTEM results, we built two Ti_nO_{2n-1} (n=6) superstructures by removing either (101) or (103) layers of O atoms in the anatase structure. In analogy with the Ti_nO_{2n-1} Magnéli phases of rutile, the microstructure of the two superstructures consists of alternate slabs of oxidized (TiO_2) and reduced (TiO) stoichiometry (see Figure 2), but extra Ti interstitials can be easily accommodated. In fact, DFT results indicate that phases of Ti_7O_{11} stoi-

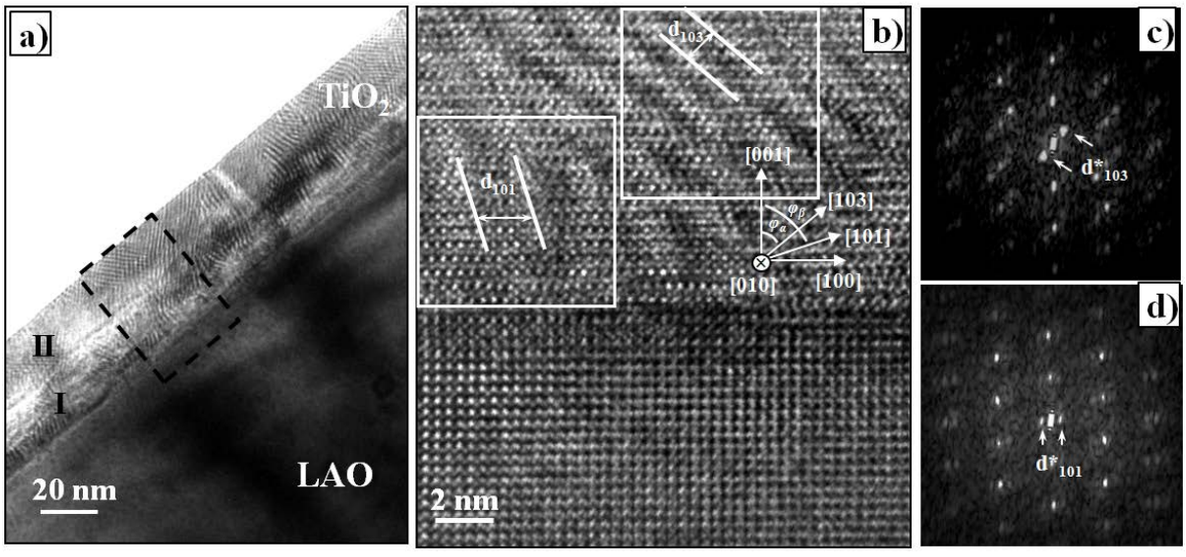

Figure 1. (a) Bright field TEM image of the TiO_2/LAO film in the [010] TiO_2 zone axis showing the splitting of the film into adjacent regions (I and II) with different diffraction contrast. (b) HRTEM image of the TiO_2/LAO interfacial region, taken in the [010] zone axis, of the film showing the presence of two types of modulations characterized by different spacing (d_{101} and d_{103}). Diffractograms taken over the region containing (c) (103) and (d) (101) CS planes. The satellite peaks around the (000) reflection are indicated by arrows in the two diffractograms.

chiometry are particularly favored. Nevertheless, the latter is preferentially formed in the region close to the interface due to the smaller lattice mismatch with substrate (Ciancio *et al.*, 2012). It is remarkable that the separation between the two CS regions coincides with the critical thickness, t ~20 nm, at which the growth mode of the TiO_2 films changes.

We used the optimized structural models described above to simulate HRTEM images of the two CS regions directly comparable to the experimental ones. Figure 3a shows a HRTEM image focused at the (103) CS region. Through-focus/through-thickness series of images were calculated for a range of crystal thickness and TEM objective lens defocus values in the [001] zone axis of the modeled structures. By matching the characteristics of the experimental images with these simulations, it was possible to find the thickness/defocus window in which the details of the CS planes are reproduced by the simulation. The best image matching was obtained at 6 nm thickness and 74-nm underfocus values. We draw attention to the following special features of the images, which have been considered important for image matching:

- Brighter contrast fringes occur at the CS planes. These have approximately 1.3 nm spacing and are inclined 38° with respect to the [100] direction of the anatase film.
- Dark low-contrast is observed between the CS planes.
- The most intense white spots occur midway within the CS planes.

The good agreement between the resulting simulated image (Figure 3b) and the experimental one confirms that the structure of the film is well described by the theoretical model. The line profiles across the intensity maxima measured along the relevant segments in the experimental and simulated images are shown in Figure 3c,d, respectively.

The comparison between the HRTEM experimental image and the simulated image of the (101) CS model is shown in Figure 4. Although the orientation and spacing of the (101) CS planes in the theoretical model agree with the experimental ones, a discrepancy is observed in the linear arrangement of the brighter contrast spots running along the long vector of the monoclinic model cell, which coincides with the [100] anatase direction. Indeed, line scan profiles taken across the intensity maxima in the simulated image show a discontinuous spacing between the bright contrast spots, whereas in the HRTEM image the intensity maxima constantly repeat over distances comparable to the long vector of the monoclinic cell. Such a discrepancy may be related to the Al interdiffusion between the substrate and the film region that we measured over the first 20 nm of the films by scanning TEM and HAADF and Energy dispersive spectroscopy.

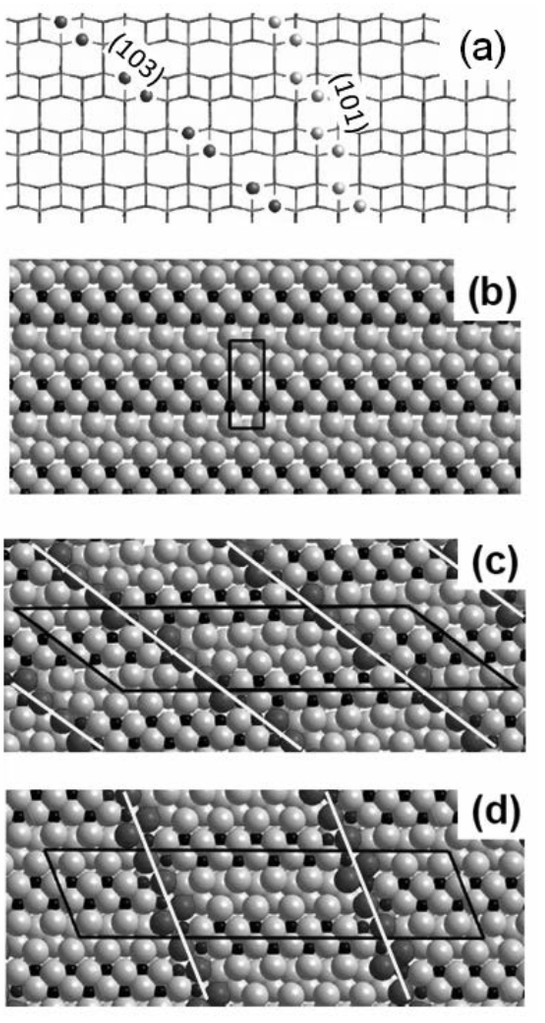

Figure 2. (a) wire-frame model of the anatase-TiO_2 structure viewed down the [010] direction; the O atoms removed in the formation of a (103) and (101) CS plane are highlighted in the structure. (b)–(d) Ball models of the anatase- TiO_2 structure and of the Ti_6O_{11} optimized superstructures formed by (103) and (101) CS planes, respectively. All structures are viewed down the [010] anatase direction. White lines indicate CS planes, and black lines indicate the projected unit cell, *i.e.*, the conventional body-centered tetragonal cell for anatase and the base-centered monoclinic cells for the superstructures. Large and small spheres are oxygen and titanium ions, respectively. Ions at the CS planes are shown in color to highlight the local structure.

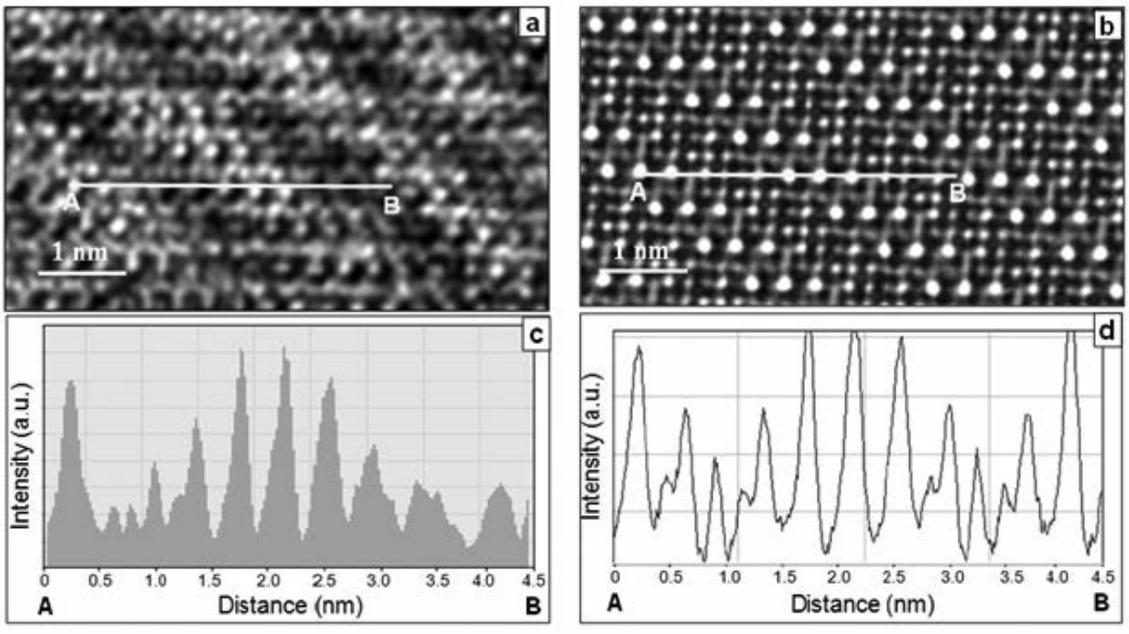

Figure 3. (a) HRTEM image focused at the film region containing (103) shear planes and taken in the [010] zone axis of the anatase film. (b) Simulated image obtained from the (103) CS modeled structure obtained at 6 nm thickness and 74-nm underfocus values. Line scans across image intensity maxima calculated along the line of the (c) experimental and (d) simulated image.

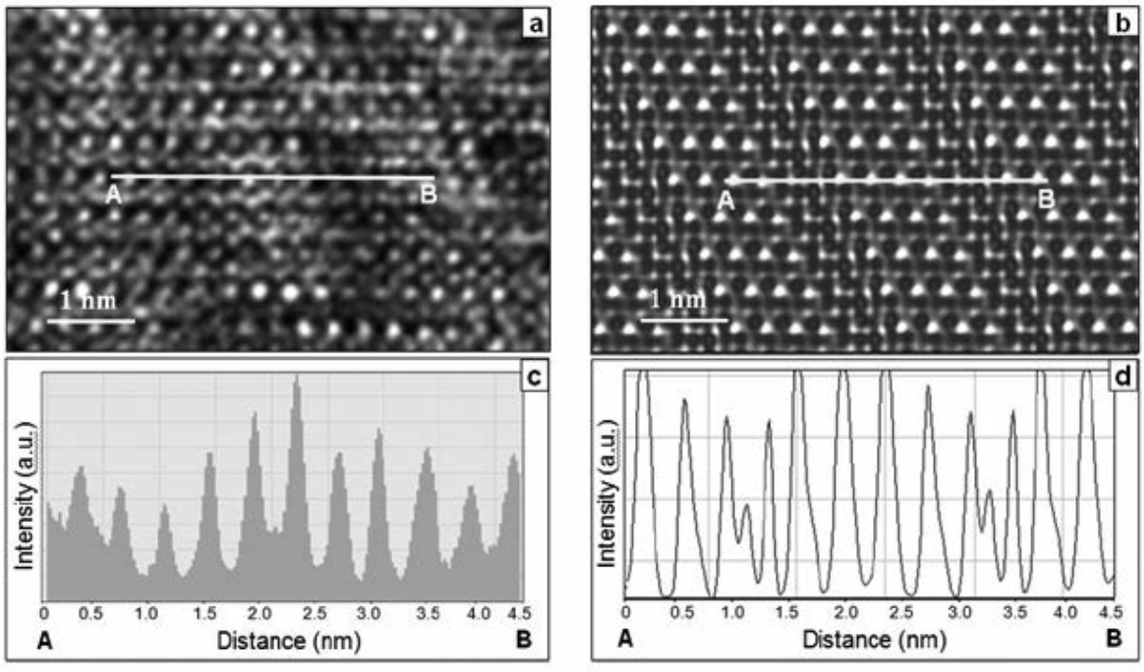

Figure 4. (a) HRTEM image focused at the film region containing (101) shear planes and taken in the [010] zone axis of the anatase film. (b) Image simulation calculated from the (101) CS modeled structure obtained at 6 nm thickness and 74-nm underfocus values. Line scans across phase maxima calculated along the line of the (c) experimental and (d) simulated image.

Figure 5 shows a typical HAADF-STEM image of the TiO_2/LAO interfacial region. Contrast variations are seen between the two slabs of the film. Since STEM dark field experiments produces images whose contrast is approximately proportional to the square of the average atomic number of the illuminated area (brighter contrast being associated with heavier elements), we can conclude that the region close to the substrate has a higher density compared to the outer region of the film. EDS analysis performed across the overall film/substrate interfacial region reveals indeed an Al diffusion from the substrate towards the film which runs out after the first 20 nm. Cationic interdiffusion has been observed also in TiO_2 anatase thin films deposited on $SrTiO_3$ substrates and has been addressed as a consequence of a peculiar reactivity of TiO_2 anatase with perovskite substrates (Ciancio, 2012b). The observation of a (101) CS-like structure in the region closest to the interface poses intriguing questions on the formation energies of the shear structures in relation with the growth modes of the film and on the capability of the (101) CS structure in driving Al^{3+} ions diffusion below the critical thickness of the film. The elucidation of the structure of the (101) CS region close to the interface requires, in addition to the work done for the pure phase, the determination of the density of Al impurities and their localization. This refinement is a work in progress and represents a challenge for future investigations.

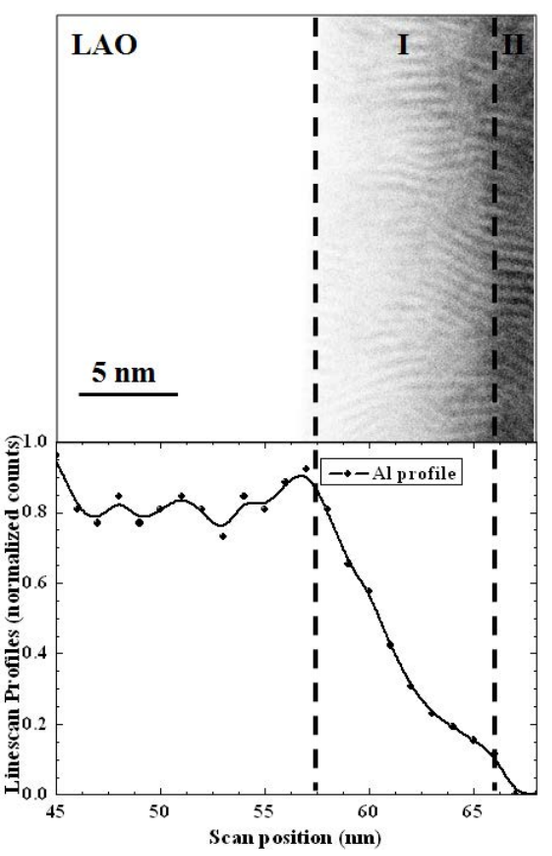

Figure 5. (Upper panel) HAADF/STEM image of the TiO_2/LAO interfacial region. (Lower panel) EDS elemental profile of Al acquired on the area displayed in the image.

Conclusions

In summary, we investigated the nanostructural arrangement of anatase TiO_2 thin films on LAO substrates. HRTEM, HAADF and EDS analyses unveiled the existence of two different types of defective regions within the film nanostructure characterized by interdiffusion phenomena connected to a peculiar reactivity of TiO_2 with perovskite substrates. By combining image simulations and first principle calculations, we demonstrated that both consist of defective phases of TiO_2 anatase with Ti_6O_{11} stoichiometry, each characterized by shear planes with different crystallographic orientation and interstitial Ti inclusions. Their microstructure consists of alternate slabs of anatase and of $[Ti_2O_3]$ blocks, resembling the Magnéli phases of rutile. We investigated the phase diagrams of these structures, determining their stability vs. alternative defective structures at different Oxygen chemical potentials. The results allowed to understand how (103) CS are prevalent in the film bulk, while (101) are mostly observed close to the interface with the substrate due to a better epitaxial matching. These results pave the way towards the optimization of manufacturing technologies based on anatase by the control of oxygen vacancies and to the technological application of Magnéli phases in anatase.

Acknowledgments

We thank E. Cociancich for the assistance in the TEM specimen preparation. R.C.'s research activity has received funding from the European Community's Seventh Framework Programme 2007-2011 under grant agreement no.212348 NFFA and Progetto strategico NFFA (fondi-MIUR).

References

Anisimov VI, Zaanen J, Andersen OK. Band theory and Mott insulators: Hubbard U instead of Stoner I. Phys Rev B 1991;44:943-54.

Carlino E, in Beam Injection Based nanocharacterization of advanced materials, ed. Salviati G, Sekiguchi T, Heun S, Gustafsson A, Research Signpost 37/661 Fort P.O. Trivandrum-695 023, Kerala, India, 2008, p. 237.

Chambers SA. Epitaxial growth and properties of doped transition metal and complex oxide films. Adv Mater 2010;22:219-48.

Chambers SA, Wang CM, Thevuthasan S, Droubay T, McCready DE, Lea AS. Epitaxial growth and properties of MBE-grown ferromagnetic Co-doped TiO2 anatase films on SrTiO3(001) and LaAlO3(001). Thin Solid Films 2002;418:197-210.

Chang HLM, You H, Guo J, Lam DJ. Epitaxial TiO2 and VO2 films prepared by MOCVD. Appl Surf Sci 1991;4849:12-8.

Chen JP, Yang RT. Selective Catalytic Reduction of NO with NH3 on SO−24/ TiO2 Superacid Catalyst. J Catal 1993;139:277-88.

Chen G, Bare SR, Mallouk TE. Development of supported bifunctional electrocatalysts for unitized regenerative fuel cells. J Electrochem Soc 2002;149: A1092-9.

Ciancio R, Carlino E, Rossi G, Aruta C, Scotti di Uccio U, Vittadini A, et al. Magnéli-like phases in epitaxial anatase TiO2 thin films, Phys Rev B 2012;86:104110.

Ciancio R, Carlino E, Aruta C, Maccariello D, Granozio FM, Scotti di Uccio U. Nanostructure of buried interface layers in TiO2 anatase thin films grown on LaAlO3 and SrTiO3 substrates. Nanoscale. 2012;4:91-4.

Cococcioni M, deGironcoli S. Linear response approach to the calculation of the effective interaction parameters in the LDA+U method. Phys Rev B 2005; 71:035105.

Ganduglia-Pirovano MV, Hofmann A, Sauer J. Oxygen vacancies in transition metal and rare earth oxides: Current state of understanding and remaining challenges. Surf Sci Rep 2007;62:219270.

Giannozzi P, Baroni S, Bonini N, Calandra M, Car R, Cavazzoni C, et al. QUANTUM ESPRESSO: a modular and open-source software project for quantum simulations of materials. J Phys Condens Matter. 2009;21:395502.

Henrich VE, Cox PA. The surface science of metal oxides, Cambridge University Press, Cambridge, 1994.

Jellison GE, Modine FA Boatner LA. Measurement of the optical functions of uniaxial materials by two-modulator generalized ellipsometry: rutile (TiO2). Opt Lett 1997;22:1808-10.

Kennedy RJ, Stampe, PA. The influence of lattice mismatch and film thickness on the growth of TiO2 on LaAlO3 and SrTiO3 substrates. J Cryst Growth 2003;252:333-42.

Lazzeri M, Vittadini A, Selloni A. Structure and energetics of stoichiometric TiO2 anatase surfaces. Phys Rev B 2011;63:155409.

Lotnyk A, Senz S, Hasse D. Epitaxial growth of TiO2 thin films on SrTiO3, LaAlO3 and yttria-stabilized zirconia substrates by electron beam evaporation. Thin Solid Films 2007;515:3439-47.

Marzari N, Vanderbilt D, De Vita A, Payne MC. Thermal contraction and disordering of the Al(110) surface. Phys Rev Lett 1999;82:3296.

Murakami M, Matsumoto Y, Nakajima K, Makino T, Segawa Y, Chikyow T, et al. Anatase TiO2 thin films grown on lattice-matched LaAlO3 substrate by laser molecular-beam epitaxy. Appl Phys Lett 2001; 78:2664-6.

Perdew JP, Burke K, Ernzerhof M. Generalized gradient approximation made simple. Phys Rev Lett 1996; 77:3865-8.

Rao CNR, Raveau B. Transition Metal Oxides: Structure, properties, and synthesis of ceramic oxides 2nd ed., Wiley-VCH, New York, 1998.

Sanchez del Rìo M, Dejus RJ, XOP: Recent developments. SPIE Proc 1998;3448:340.

Stadelmann P. JEMS Electron Microscopy Software 2006, JAVA version 3.0505W2006, http://cimewww.epfl.ch/people/stadelmann/jemsWebSite/jems.html.

Szot K, Rogala M, Speier W, Klusek Z, Besmehn A, Waser R. TiO2-a prototypical memresistive material. Nanotechnology 2001;22:254001.

Yamamoto S, Sumita T, Sugiharuto T, Miyashita A, Naramoto H. Preparation of epitaxial TiO2 films by pulsed laser deposition technique. Thin Solid Films 2001;401:88-93.

Wang Z, Zeng W, Gu L, Saito M, Tsukimoto S, Ikuhara Y. Atomic-scale structure and electronic property of the LaAlO3/ TiO2 interface. J Appl Phys 2010;108: 113701.

Weinberger B, Garber R. Titanium dioxide photocatalysts produced by reactive magnetron sputtering. Appl Phys Lett 1995;66:2409-11.

Weng X, Fisher P, Skowronski M, Salvador PA, Maksimov O. Structural characterization of TiO2 films grown on LaAlO3 and SrTiO3 substrates using reactive molecular beam epitaxy. J Cryst Growth 2008;310:545-50.

Windt DL. IMD- Software for modeling the optical properties of multilayer films. Comput Phys 1998;12: 360-70.